EARTH SURFACE PROCESSES AND LANDFORMS
Earth Surf. Process. Landforms **40**, 1318–1333 (2015)
Copyright © 2015 John Wiley & Sons, Ltd.
Published online 10 May 2015 in Wiley Online Library
(wileyonlinelibrary.com) DOI: 10.1002/esp.3722

Bar dynamics and bifurcation evolution in a modelled braided sand-bed river

Filip Schuurman[1,2]* and Maarten G. Kleinhans[1]
[1] Faculty of Geosciences, Department of Physical Geography, Utrecht University, The Netherlands
[2] Department of Rivers, Deltas and Coasts, Royal HaskoningDHV, Amersfoort, The Netherlands

Received 30 January 2014; Revised 28 January 2015; Accepted 9 February 2015

*Correspondence to: Filip Schuurman, Faculty of Geosciences, Department of Physical Geography, Utrecht University, PO Box 80115, 3508 TC Utrecht, The Netherlands. E-mail: f.schuurman@uu.nl

ESPL
Earth Surface Processes and Landforms

ABSTRACT: Morphodynamics in sand-bed braided rivers are associated with simultaneous evolution of mid-channel bars and channels on the braidplain. Bifurcations around mid-channel bars are key elements that divide discharge and sediment. This, in turn, may control the evolution of connected branches, with effects propagating to both upstream and downstream bifurcations. Recent works on bifurcation stability and development hypothesize major roles of secondary flow and gradient advantage. However, this has not been tested for channel networks within a fully developed dynamic braided river. A reason for this is a lack of detailed measurements with sufficient temporal and spatial length, covering multiple bifurcations. Therefore we used a physics-based numerical model to generate a dataset of bathymetry, flow and sediment transport of an 80 km river reach with self-formed braid bars and bifurcations. The study shows that bar dissection due to local transverse water surface gradients is the dominant bifurcation initiation mechanism, although conversion of unit bars into compound bars dominates in the initial stage of a braided river. Several bifurcation closure mechanisms are equally important. Furthermore, the study showed that nodal point relations for bifurcations are unable to predict short-term bifurcation evolution in a braided river. This is explained by occurrence of nonlinear processes and non-uniformity within the branches, in particular migrating bars and larger-scale backwater-effects, which are not included in the nodal point relations. Planform morphology, on the other hand, has predictive capacity: bifurcation angle asymmetry and bar-tail limb shape are indicators for near-future bifurcation evolution. Remote sensing data has predictive value, for which we developed a conceptual model for interactions between bars, bifurcations and channels in the network. We conducted a preliminary test of the conceptual model on satellite images of the Brahmaputra. Copyright © 2015 John Wiley & Sons, Ltd.

KEYWORDS: braided river; bifurcations; Bars; numerical model; Delft3D

Introduction

Braided rivers consist of a network of channels, or branches, and alluvial mid-channel bars (e.g. Leopold and Wolman, 1957). Each well-developed mid-channel bar forms a bifurcation, dividing discharge and sediment over the downstream branches. Bifurcations determine sediment availability and sediment transport capacity in the branches and thus have a major influence on the morphodynamics in braided rivers, including migration and deformation of mid-channel bars and branches. The interaction between bifurcations, branch dynamics and mid-channel bar dynamics is a challenge for river managers to deal with and for modellers to simulate but has large relevance for societies living on fluvial plains. Meanwhile, collection of detailed field data of large braided systems over long periods of time to unravel the dominant processes remains technically and financially challenging. Here we study the interaction between bifurcation evolution and bar dynamics using data of a large braided river generated in a detailed physics-based numerical model.

At least two types of bars can be distinguished in braided rivers (e.g. Rice *et al.*, 2009) (Figure 1). Unit bars (Figure 1c) are the simplest type of bars, characterized by a lobed planform, relatively high downstream part with a steep downstream slip-face, and submerged during average discharge. They maintain their general shape during migration. Compound bars are larger, more complicated bars formed by merging of unit bars (Figure 1a, b). Typically, compound bars form bifurcations and confluences, whereas unit bars are too low for this. Upstream erosion of compound bars, commonly accompanied by an increase of bifurcation angle, provides sediment that is (partly) deposited at the downstream end of the bar, forming shallow bar-tail limbs (Figure 1b) (Leopold and Wolman, 1957; Bridge, 1993; Best *et al.*, 2006; Ashworth *et al.*, 2000). Agglomeration of bars can form large bar complexes (Sambrook Smith *et al.*, 2006), with, for example, reported lengths in the Brahmaputra exceeding 15 km (Ashworth *et al.*, 2000) and 30 km (Bristow, 1993).

The initiation and closure of bifurcations in braided rivers is directly linked with the bar dynamics: agglomeration of bars occurs with bifurcation closure, and bar dissection occurs with bifurcation initiation. Bifurcation initiation in a braided rivers occurs by over-bar flow forming cross-bar channels, and eventually a mature branch (Figure 1a). In a mildly braided

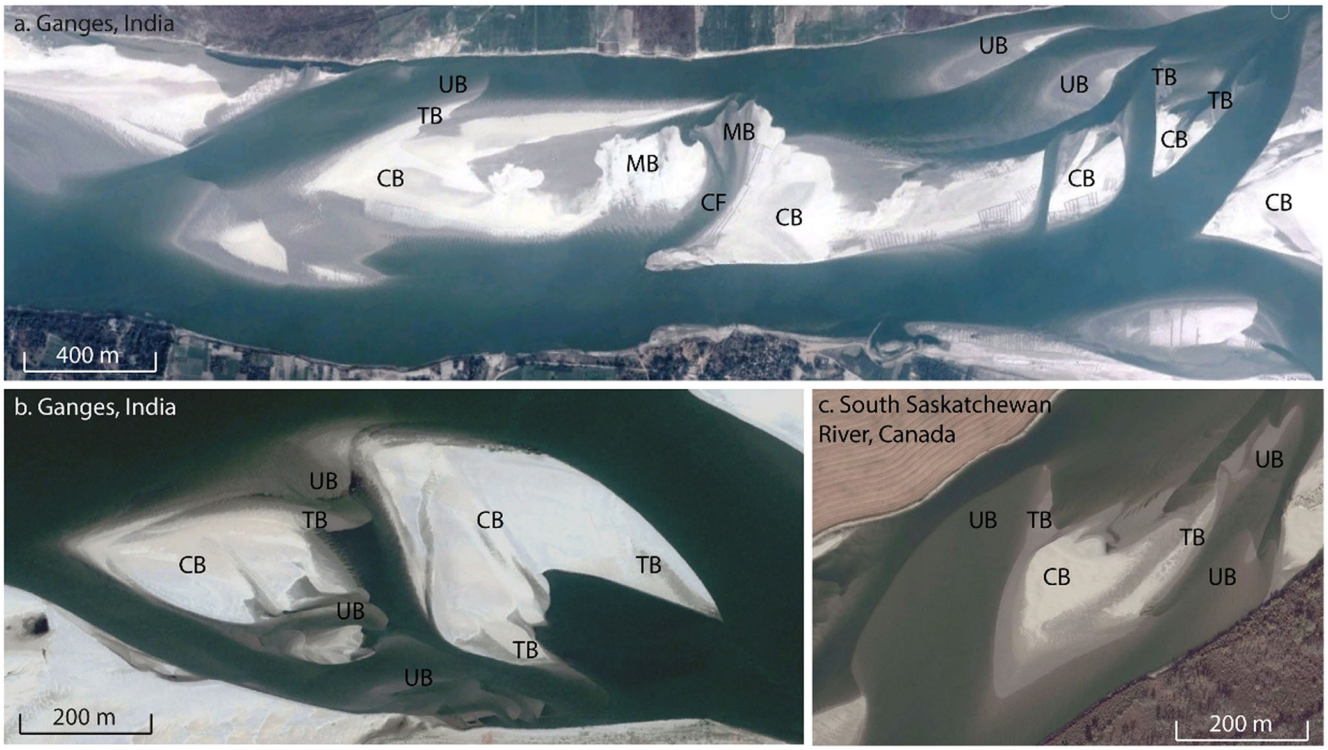

Figure 1. Examples of mid-channel bars in the Ganges and the South Saskatchewan River, with compound bars (CB), unit bars (UB), bar-tail limbs (TB), mouth bars (MB) and bar dissection by a cross-bar channel (CF). Flow is from left to right. Source: GoogleEarth (a, b) and BingMaps (c). This figure is available in colour online at wileyonlinelibrary.com/journal/espl

river, chute cutoffs of bank-attached bars also contribute significantly to the formation of new branches. At the same time, bifurcations in braided rivers are often so unstable and asymmetrical that only one of the branches is usually dominant (Bertoldi *et al.*, 2009; Egozi and Ashmore, 2008; Marra *et al.*, 2013), emphasizing the key role that bifurcations play in discharge division. Indeed, Marra *et al.* (2013) found that only one or two dominant branches occur in the Jamuna River, depending on the reach, and that changes were much more rapid in less dominant branches. So, for understanding and predicting short-term evolution of a bifurcation in a braided river, it is important to regard bifurcations as being a piece of a network of branches.

Relatively simple analytical predictors exist for individual bifurcation evolution, based on the difference in channel dimensions of two bifurcation branches (Wang *et al.*, 1995; Bolla Pittaluga *et al.*, 2003; Kleinhans *et al.*, 2008, 2013). These predictors basically consist of three steps: (i) prediction of discharge division; (ii) prediction of sediment transport division; and (iii) prediction of bed-level change in the branches. Although these predictors highly simplify the detailed processes of flow and sediment partitioning at the bifurcations as also acknowledged by the authors, tests on experiments, on model data in an idealized bifurcation and on field data were successful (Bolla Pittaluga *et al.*, 2003; Kleinhans *et al.*, 2008, 2013). Thus these models provide a method to predict bifurcation evolution, and thus potentially short-term braided river evolution, based on a few characteristic parameters. For example, the width ratio of two bifurcation branches could be an indicator for the discharge and sediment division, which is useful when only aerial photos are available. Here we test these predictors for a braided river.

Others used the bifurcation planform to predict bifurcation evolution in braided rivers. For example, Koomen (1992) found a correlation between bifurcation angle asymmetry and short-term bifurcation evolution in the Brahmaputra. In particular, he found a more frequent occurrence of branch abandonment for branches with a larger bifurcation angle deviation from the upstream branch. Although flume experiments of Federici and Seminara (2003) and numerical modelling by Van der Mark and Mosselman (2012) indicated no correlation between bifurcation angle asymmetry and bifurcation evolution, it is a plausible correlation and deserves further investigation. Furthermore, Koomen (1992), Ashworth *et al.* (2000) and Schuurman *et al.* (2013) found that the relative length of bar-tail limbs is an indicator of bifurcation asymmetry, and thus short-term evolution: the dominant channel creates the longest bar-tail limb. In accordance with this, Best *et al.* (2003) provided an example of a mid-channel bar where the asymmetrical growth was related to dominance of either branch. Despite the potential of both the bifurcation angle asymmetry and length of bar-tail limbs being indicators for short-term bifurcation evolution, they are based on single bifurcations and do not reflect the effects of the network aspect and interactions with other bifurcations and bars.

Field observations and flume experiments are essential to understand braided rivers. However, they have not yet provided a dataset of sufficient spatial and temporal resolution and length to analyse the interaction between the complicated flow, sediment transport, bar dynamics and bifurcation evolution in large braided rivers, or to analyse the poorly understood interaction between multiple adjacent bifurcations and bars (Ferguson, 1993; Kleinhans *et al.*, 2013). Therefore, Nicholas (2013a) and Schuurman *et al.* (2013) applied physics-based numerical modelling to produce 'datasets' of braided rivers, and analysed bar and branch dynamics in these representations of real rivers, taking into account the network aspect. Many general characteristics of braided rivers and their dynamics were reproduced in these models. Although the models are highly sensitive to constitutive relations for bed roughness, sediment transport relation and bed slope effect, they enable analysis of braided river morphodynamics with control of initial and boundary conditions, and with temporal and spatial resolutions, length and duration that surpass

Copyright © 2015 John Wiley & Sons, Ltd.

the current capability of field measurements. Thus they enable analysis of bifurcations and bars taking into account the network aspect.

From the above the following main questions addressed in this paper emerge: (i) how do bifurcations control the near-future evolution of downstream bars and branches in large sand-bed braided rivers? (ii) how, in turn, does the evolution of bars and branches control the division of water and sediment at nearby bifurcations? This feedback loop leads to the question: (iii) what bar–bifurcation–branch interactions control the braiding intensity and dynamic equilibrium topography in large sand-bed braided rivers? And finally, (iv) how predictable is the near-future evolution of bifurcations in large sand-bed braided rivers?

To answer these questions: (i) we identified dominant mechanisms involving bifurcation and bar evolution in a sand-bed river; (ii) we assessed the performance of simple relations based on the dimensions of bifurcation branches and planform to predict near-future bifurcation evolution and bar dynamics; and (iii) we developed a conceptual model for bar, channel and bifurcation evolution in large sand-bed braided rivers. To these ends, we employed a 'dataset' of a braided river produced in a numerical model, because this has completely controlled boundary conditions and eliminates natural effects of vegetation, grain size variation and non-uniformity of bank material. Furthermore, we used parsimonious initial conditions and a straight braidplain to exclude the effect of topographic forcing. We compared the resulting bed morphology and dynamics to empirical relations for bar shapes and generic observations in nature and flumes. Also, we tested the conceptual model and planform-based predictors on a 25 km section of the Brahmaputra River.

Model Descriptions and Methods

Nodal point relations

Bifurcations can be symmetrical or asymmetrical, which refers to the difference in discharge between the two downstream branches. A bifurcation is in morphological equilibrium when the sediment transport capacity equals the upstream sediment delivery partitioned at the bifurcation. This equilibrium may be unstable depending on sediment mobility and channel aspect ratio (Wang *et al.*, 1995; Bolla Pittaluga *et al.*, 2003). As sediment transport capacity is a nonlinear function of flow velocity (e.g. $q_s \propto U^{3-5}$), a small adjustment of flow division at a bifurcation has a large impact on sediment transport capacity of the downstream branches.

We applied two analytical nodal point relations to predict the divisions of discharge and two relations for the division of sediment at a bifurcation, and tested these in the more complicated setting of our three-dimensionally modelled braided river. The first flow relation is based on the Chezy equation, which assumes uniform steady flow. Alternatively, the flow can be determined from an empirical hydraulic geometry relation between channel width and flow discharge, which is usually done in cases where flow depth and resistance are unknown but width can easily be observed. For the sediment division we use first the Wang *et al.* (1995) nodal point relation for the division of sediment. The second sediment division relation was adapted from Bolla Pittaluga *et al.* (2003) and was developed for gravel-bed river bifurcations. We used both sediment division relations with both flow relations and with the flow observed in the three-dimensional model, which results in six combinations that predict sediment division, which we compare to the true division observed in the three-dimensional model.

The first flow relation uses the Chezy equation to predict discharge division in a Y-shape bifurcation, assuming uniform conditions within the branches:

$$\frac{Q_3}{Q_2} = \frac{W_3}{W_2}\frac{C_3}{C_2}\left(\frac{h_3}{h_2}\right)^{\frac{3}{2}}\left(\frac{S_3}{S_2}\right)^{\frac{1}{2}} \tag{1}$$

where Q_i is the discharge to branch i ($m^3\ s^{-1}$), W_i is the channel width (m), C_i is the Chezy bed roughness ($m^{0.5}\ s^{-1}$), h_i is the water depth (m) and S_i is the water surface slope. In this relation, branch $i = 1$ is the upstream inflow channel and $i = [2, 3]$ are the downstream branches. Mass conservation applies: $Q_1 = Q_2 + Q_3$.

In the numerical model, the required variables for Equation (1) can be determined in great detail but these are often lacking in nature, for example when only satellite images are available (Bertoldi, 2012). In this case the relation between channel width and discharge ($W \propto \sqrt{Q}$) can be used to estimate the discharge division:

$$\frac{Q_3}{Q_2} = \left(\frac{W_3}{W_2}\right)^2 \tag{2}$$

where again mass conservation should apply.

The first relation we applied for sediment division uses a constitutive relation postulated in Wang *et al.* (1995):

$$\frac{Q_{s3}}{Q_{s2}} = \left(\frac{Q_3}{Q_2}\right)^k \left(\frac{W_3}{W_2}\right)^{1-k} \tag{3}$$

in which Q_{si} is the sediment transport rate ($m^3\ s^{-1}$) and k is an empirically derived constant. Here the width-averaged sediment transport rate $q = Q/W$ and $q_s \propto q^5$ for the Engelund–Hansen sediment transport predictor, which we also use in the three-dimensional model. Mass conservation of sediment applies, i.e. $Q_{s1} = Q_{s2} + Q_{s3}$. A bifurcation is stable if $k > 5/3$, as in that case Q_{s3}/Q_{s2} is more sensitive to Q_3/Q_2 than the sediment transport capacity. Thus an increase in discharge towards one of the branches results in deposition in that branch and consequently an increase of discharge and sediment transport towards the other branch. A bifurcation is unstable if $k < 5/3$. We used $k = 5/3$.

The second relation is that of Bolla Pittaluga *et al.* (2003), which initially assumes a sediment division by $k = 1$, which means that it is linearly proportional to the widths of the downstream branches:

$$\frac{Q_{s3}}{Q_{s2}} = \frac{Q_3}{Q_2} = \frac{W_3}{W_2} \tag{4}$$

This sediment flux division is modified by the transverse bed slope effect, which causes a transverse sediment flux just upstream of the bifurcation:

$$\frac{Q_{s3}}{Q_{s2}} = \frac{W_3}{W_2} + \alpha_w W_1 q_{sy} \tag{5}$$

where α_w is the multiplier on width that sets the upstream influence length of a transverse slope between the entrances of branches 2 and 3, and q_{sy} is the unit transverse sediment transport ($m^2\ s^{-1}$) due to the transverse bed slope:

$$q_{sy} = \frac{Q_{s1}}{W_1}\left(\sin(\phi_s) - f(\theta)\frac{\partial z_b}{\partial \eta}\right) \tag{6}$$

Copyright © 2015 John Wiley & Sons, Ltd.

in which η is the coordinate perpendicular to the depth-averaged flow direction and z_b is the bed surface level (m). To be consistent with the three-dimensional model the $f(\theta)$ depends on Shields parameter θ:

$$f(\theta) = \frac{1}{\alpha\theta^{\beta}} \tag{7}$$

Here, α and β are calibration parameters. Following Schuurman *et al.* (2013), we applied $\alpha = 0.7$ and $\beta = 0.5$. Furthermore, ϕ_s is the sediment transport deflecting angle from the depth-averaged flow velocity direction by helical flow which was added to the Bolla Pittaluga *et al.* (2003) model by Kleinhans *et al.* (2008):

$$\tan(\phi_s) = -A\frac{h}{R} \tag{8}$$

where R is the radius of the local streamline curvature (m) and h is the water depth (m). Here A is a helical flow coefficient assuming a logarithmic vertical flow velocity profile computed by

$$A = \frac{2}{\kappa^2}\left(1 - \frac{\sqrt{g}}{\kappa C}\right) \tag{9}$$

where κ is the Von Karman constant (0.4). The combined nodal point relation of Bolla Pittaluga *et al.* (2003) and Kleinhans *et al.* (2008) to compute sediment transport division is hereinafter referred to as BK. Note that the nodal point relations are based on simplified conditions of a Y-shape bifurcation, with uniform channel width, water depth and bed roughness within each branch. Also, flow in the branches and at the bifurcation is highly simplified as the three-dimensional flow structures in the vicinity of a bifurcation are neglected.

Numerical three-dimensional model

In this study, we used a self-formed braided river topography produced in the physics-based numerical model Delft3D building on our earlier work (Schuurman *et al.*, 2013). The hydrodynamics are computed by applying conservation of momentum in the horizontal directions (Equations (10)—(11)) and mass in horizontal and vertical directions (Equation (12)), assuming hydrostatic pressure:

$$\begin{aligned}\frac{\partial u}{\partial t} + u\frac{\partial u}{\partial x} + v\frac{\partial u}{\partial y} + w\frac{\partial u}{\partial z} &= -g\frac{\partial z_w}{\partial x} - \frac{gu\sqrt{u^2+v^2}}{C^2 h} \\ &+ V_h\left(\frac{\partial^2 u}{\partial x^2} + \frac{\partial^2 u}{\partial y^2}\right) + \frac{\partial}{\partial z}\left(V_v\frac{\partial u}{\partial z}\right)\end{aligned} \tag{10}$$

$$\begin{aligned}\frac{\partial v}{\partial t} + u\frac{\partial v}{\partial x} + v\frac{\partial v}{\partial y} + w\frac{\partial v}{\partial z} &= -g\frac{\partial z_w}{\partial y} - \frac{gv\sqrt{u^2+v^2}}{C^2 h} \\ &+ V_h\left(\frac{\partial^2 v}{\partial x^2} + \frac{\partial^2 v}{\partial y^2}\right) + \frac{\partial}{\partial z}\left(V_v\frac{\partial v}{\partial z}\right)\end{aligned} \tag{11}$$

$$\frac{\partial(hu)}{\partial x} + \frac{\partial(hv)}{\partial y} + \frac{\partial w}{\partial z} = 0 \tag{12}$$

where x is the downstream coordinate (m), y is the lateral coordinate (m), z is the vertical coordinate (m), z_w is the water surface level (m), u is the flow velocity in the x-direction (ms^{-1}), v is the flow velocity in the y-direction (ms^{-1}), w is the flow velocity in the z-direction (ms^{-1}), h is the water depth (m), C is the Chezy roughness ($m^{0.5}s^{-1}$), g is the gravity acceleration constant (ms^{-2}), V_h is the horizontal eddy viscosity (m^2s^{-1}) and V_v is the vertical eddy viscosity (m^2 s^{-1}). A detailed description of the hydrodynamics and numerical scheme of Delft3D can be found in Lesser *et al.* (2004), Van der Wegen and Roelvink (2008) and Deltares (2009).

The morphodynamics in Delft3D result from sediment transport, bed slope effects, bank erosion and mass conservation in the bed. The sediment transport rate in each grid cell is equal to the sediment transport capacity calculated according to Engelund and Hansen (1967):

$$q_s = \frac{0.05U^5}{\sqrt{g}C^3\Delta^2 D_{50}} \tag{13}$$

where q_s is the total sediment transport per unit width (m^2 s^{-1}), U is the depth-averaged flow velocity in streamline direction (m s^{-1}), Δ is the non-dimensional relative mass density of sediment underwater and D_{50} is the median grain size (m). At the upstream boundary the amount of upstream sediment inflow was equal to the local sediment transport capacity which keeps the bed level constant. The transverse bed slope effect, which is the downslope pulling of sediment by gravity and essential in morphodynamic models (e.g. Struiksma *et al.*, 1985; Talmon *et al.*, 1995; Schuurman *et al.*, 2013), is computed according to Koch and Flokstra (1981). After each time step, the bed level was updated using the Exner equation. To reduce computational time, an acceleration factor of 25 was used for bed-level change on the basis of spatial sediment transport gradients, which is allowed because morphology changes much more slowly than hydrodynamics. The chosen acceleration has no significant effect on morphology (Roelvink, 2006; Schuurman *et al.*, 2013).

Sediment transport was only calculated above threshold water depths of 0.1 m. Grid cells with smaller water depth were considered to be inactive. Inactive grid cells reactivated when the threshold water depth was exceeded, either by water-level rise or by a simplified formulation of bank erosion. Here, 'bank erosion' of a dry grid cell occurred when a neighbouring wet grid cell eroded, where 50% of the incision in the wet cell was applied to the dry cells (Van der Wegen and Roelvink, 2008). This prevents unnatural effects of accidentally emerged cells. Test runs showed that the resulting morphology is insensitive to the bank erosion percentage (see Figure C of the online supplementary material).

Table I. Initial and boundary conditions

Parameter	Unit	Run 1	Run 2
Discharge	m^3 s^{-1}	20 000	40 000
Channel width	m	3200	3200
Channel length	m	80 000	80 000
Bed slope	—	9.30×10^{-5}	9.30×10^{-5}
D_{50}	m	2.00×10^{-4}	2.00×10^{-4}
Constant k_s	m	0.15	0.15
Initial water depth	m	5.7	8.6
Initial Froude number	—	0.15	0.16
Initial Shields number	—	1.61	2.42
Grid cell length × width	m	50 × 20	50 × 20
Sediment transport predictor	—	EH	EH
Perturbation max. init. bed level	m	0.01	0.01
Perturbation period of Q	days	2.28	2.28
Perturbation SD amplitude of Q	%	0.5	0.5
Hydrodynamic time step	s	6	6
Morphodynamic time step	s	150	150

Copyright © 2015 John Wiley & Sons, Ltd.

Model settings and boundary conditions for the three-dimensional numerical model

The simulated river had a straight, initially plane, bed of 3200 m width and 80 km length with a uniform initial bed slope of 9.3×10^{-5} and uniform fine sand (D_{50} = 200 μm) (Table I). The model schematisation and input files are provided in the online supplementary material. The channel had fixed non-erodible walls and a movable bed. Two different constant discharges were modelled: 20 000 m^3 s^{-1} (run 1) and 40 000 m^3 s^{-1} (run 2). The predicted design braiding index BI based on Crosato and Mosselman (2009) was 8 for run 1 and 6 for run 2.

The computational domain was discretized by 50 m × 20 m grid cells, and the water column was divided into seven grid cells with boundaries at constant fractions of the water depth (so called σ-grid). Thus vertical grid resolution was relatively high at low water depths. The length of the grid cells was 2.5 times the grid cell width, in order to keep the aspect ratio around 2 and to optimize speed at the same time. Note that we used a 16 times higher horizontal grid resolution than Schuurman *et al.* (2013), and seven instead of one vertical grid layer.

The hydraulic boundary conditions consisted of a constant upstream inflow and a fixed downstream water level. The upstream boundary was split into 20 separate boundary sections, i.e. eight grid cells per boundary section. For each boundary section, the amount of inflow was defined in a time series. The water level at the downstream boundary was based on initial uniform flow conditions. The duration of the runs was at least 27 months. The hydrodynamic time step was 6 s, so the morphodynamic time step was 150 s given a morphological factor of 25.

Although bed roughness in natural rivers varies spatially due to the presence of bed forms, we applied a constant uniform bed roughness following Nicholas (2003), Lesser *et al.* (2004) and Schuurman *et al.* (2013), assuming that bed forms such as dunes were subgrid. Nicholas *et al.* (2012) showed that spatial variation of bed roughness does not significantly improve model results. In this study we used a uniform Nikuradse k_s of 0.15 m.

As bars form in response to a forcing or perturbation and need continuous perturbation to retain dynamics (e.g. Van Dijk *et al.*, 2012), perturbations were applied to the upstream inflow and initial bed surface, similar to applied by Schuurman *et al.* (2013). The upstream inflow perturbation was a random time-varying and spatial-varying noise added or subtracted to the inflow at each of the 160 m wide upstream boundary sections. It had a standard deviation of 0.5% of the boundary section inflow and changed every 2.3 days. The initial bed level perturbation was spatially varying with a maximum of 1 cm added to or subtracted from the initially smooth bed in each grid cell. This perturbation was a maximum 2.4% of the initial water depth. As these perturbations had a much shorter time and spatial scale than the bars, they were considered noise rather than forcing.

Methods of analysis

The analysis consisted of two main parts: (i) braided river dynamics including initiation of mid-channel bars and bifurcations, and the evolution of the reach-scale channel network; and (ii) evolution and predictability of bifurcations in combination with bar and channel dynamics.

The first part is based on the recorded time series of the modelled bed level, sediment transport and hydrodynamics. We identified initiation and closure mechanisms for the bifurcations, and compared the shape of the bars with empirical relations of Kelly (2006). We described the bar shape by using ratios between metrics: (i) aspect ratio = major axis length/minor axis length; (ii) compactness = bar perimeter/bar surface area; (iii) roundness = convex hull perimeter/bar surface area. The use of such metrics and ratios is comparable to Meshkova and Carling (2013), for example. Furthermore, we computed 2D maps of lateral water surface gradient to determine its influence on bifurcation evolution after detrending water surface by the initial longitudinal bed slope.

The second part describes the short-term evolution of two bifurcations in run 2: one near river kilometre x = 25 km and one near x = 30 km. We started with testing the nodal point relations (Equations (1)–(9)). We recorded input parameters for the nodal point relations from cross-sections defined consistently with the assumptions of the relations and similar to conventional field measurement methods. Channel width, cross-sectional averaged water depth and Chezy bed roughness were recorded over transects *p2* and *p3*, perpendicular to the flow (Figure 2). Discharge and sediment divisions were recorded over two transects perpendicular to the average river gradient (*o2* and *o3* in Figure 2). Upstream flow curvature was recorded over transect *x1* at the location $\alpha_w W_1$ upstream of the bifurcation point (BP), which was automatically defined from streamlines. Transverse bed slopes were recorded over transects *o2* and *o3* at a distance of $0.5W$ upstream of BP. Water surface slopes were recorded from BP to $\alpha_w W_1$ downstream of BP. The transverse sediment transport Q_{sy} was determined along the streamline through BP, over a distance of $\alpha_w W_1$ upstream of BP. Following Bolla Pittaluga *et al.* (2003), a length of two times the channel width (α_w = 2) was used.

After this, we tested two planform-based indicators for short-term bifurcation evolution: bifurcation angle and the shape of bar-tail limbs. The bifurcation angles were recorded using the mid-channel bar edges (Figure 2), which is generally a larger angle than that of the downstream channel axes

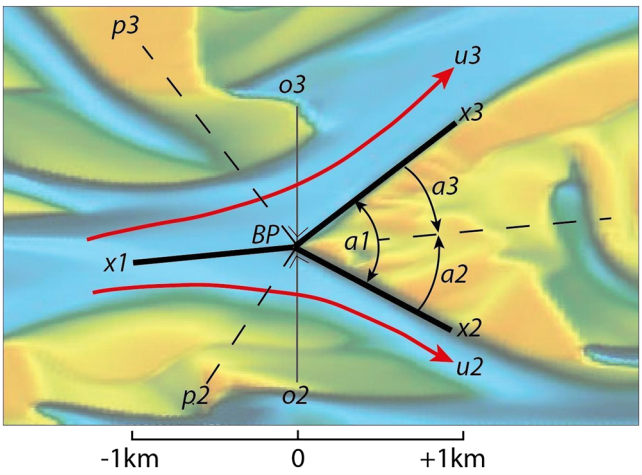

Figure 2. Definitions of the angles and transects in the vicinity of a bifurcation. The red arrows indicate streamlines into the middle of the branches; BP indicates the bifurcation point; *x*-lines define the bifurcation; *x*1 is a curved centreline of the upstream channel determined by the streamline through BP; *a*1 is the bifurcation angle, and *a*2 and *a*3 are deviation angles from inflow channel direction; *o*-lines are transects parallel to the grid *y*-axis through BP, used for measuring discharge, sediment transport and transverse bed slope; *p*-lines are transects perpendicular to *x*2 or *x*3, used for measuring the cross-sectional profiles (channel width and average water depth). This figure is available in colour online at wileyonlinelibrary.com/journal/espl

Copyright © 2015 John Wiley & Sons, Ltd.

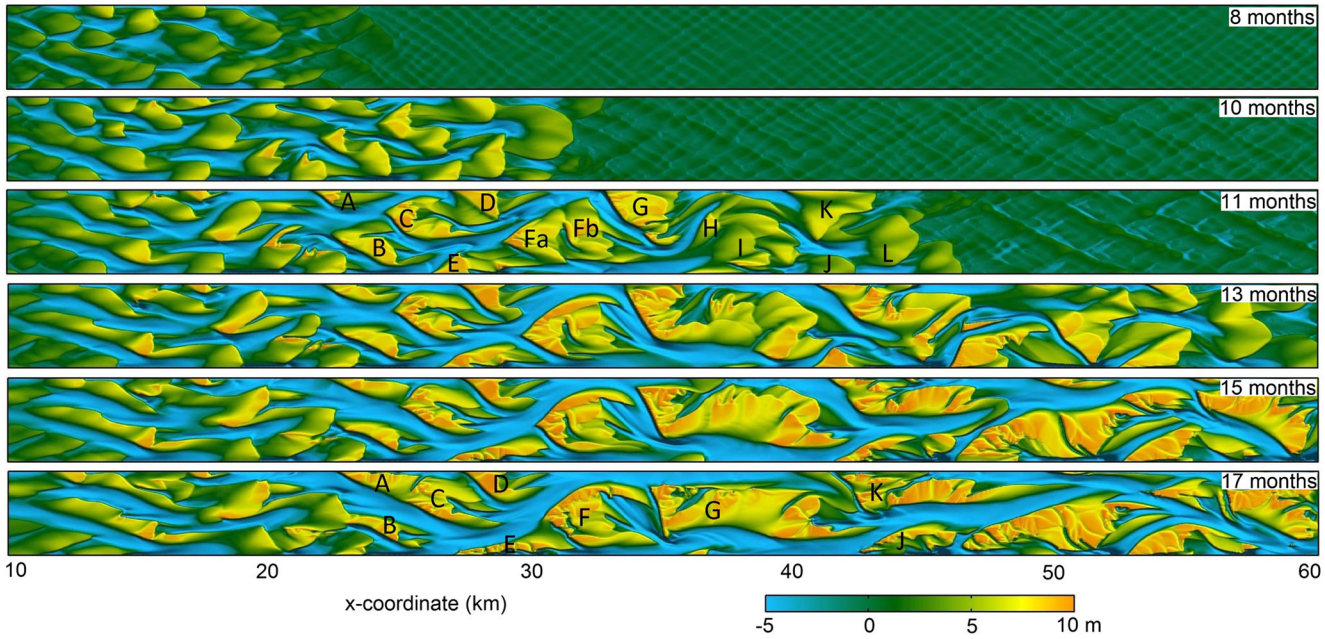

Figure 3. Initiation and evolution of a braided channel pattern in run 2. Labelled bars are referred to in Figures 4, 5, 7, 8, 11–13 and 15. This figure is available in colour online at wileyonlinelibrary.com/journal/espl

(Federici and Paola, 2003; Bertoldi and Tubino, 2005). The bifurcation angle asymmetry (a) was defined as

$$a = \frac{a3 - a2}{a1} \tag{14}$$

in which index 1 indicates the upstream inflow channel, index 2 indicates the branch with decreasing discharge and index 3 indicates the branch with increasing discharge.

The measurements were complemented by more qualitative observations of the morphodynamics, which are changing patterns with many aspects that are challenging to quantify. We classified the styles of bifurcation formation and termination and counted their frequency over the entire length and time period of the model. To avoid subjectivity the recognition and counting were performed systematically by an assistant in the MSc earth science program. Furthermore, we qualitatively analysed occurrences of bar-tail limbs and their correlation to bifurcation development.

Results

From flat bed to braided river

The development of a braided river topography from a planar bed in run 2 is shown in Figure 3. A timeseries of the development of run 1, and a movie of the developments in both runs, are given in the online supplementary. Unit bars formed at the upstream edge and migrated in a downstream direction with a celerity of around 1 km/month. These bars forced downstream formation of new bars (Figure 4). Downstream migration celerity of this bar front was around 10 km/month. At the same time, bars formed in the entire reach induced by the initial bed perturbations, although these high-mode bars aggraded slowly and were overflowed by the bars formed upstream. Simultaneously with the migration of the unit bars, the bars aggraded and flow was increasingly redirected around the high bar centre, comparable to Ashworth *et al.* (2000). The increased flow and sediment transport around the bar centre caused channelization. Now, bar-tail limbs formed at the downstream side of the bars, expanding the surface area of the bars. As the bar-tail limbs elongated, some became attached to a downstream located bar, closing the branch between both bars and causing bar merging. Consequently, flow became concentrated in 2-3 channels that occupied around 1/3 of the channel width (see Figure A of online supplementary material).

Deposition at the downstream side of the compound bars, commonly in the form of bar-tail limbs, was the result of either a decrease in sediment transport capacity in downstream direction in the lee side of a bar, causing deposition of sediment; or a decrease in sediment transport capacity of over-bar flow in the lateral direction and consequently deposition at the slip-face of the bar. The first mechanism induced elongation of the bar-tail limb, whereas the second mechanism induced widening of the bar-tail limb from the bar perimeter inward. Both mechanisms occurred at bar F (Figure 5): between month 12 and 14, the northern bar-tail limb elongated, whereas later a dead-zone and low water level caused by the bar-tail limb resulted in flow over the bar-tail limb and widening of the bar-tail limb. Also, the bar-tail limb expansion exceeded erosion rates of bar G, causing narrowing of the branch between bars F and G. The same occurred at the southern bar-tail limb of bar F. Thus sufficient flow intensity and sediment transport parallel to the bar-tail limb are crucial for bar-tail limb expansion, which is illustrated by the sudden stagnation of the northern bar-tail limb of bar C when discharge towards the branch between bars A and C decreased. Bar D is another example of bar-tail limb elongation in the direction parallel to the dominant flow between bars D and F.

The shape of the self-formed bars was similar to the bars observed in natural rivers and flume experiments by Kelly (2006) (Figure 6). Aggradation, expansion and merging of the bars resulted in a decrease in braiding intensity from around eight active parallel branches in the first month to around two active parallel branches after one year. The dominant branches had the tendency to attach to the outer channel walls, which also occurs in reaches with resistant banks in, for example, the River Irrawaddy (Myanmar) and River Ganges (India). One explanation is that the lack of bank erosion causes local incision (Ashworth *et al.*, 2000; Mosselman, 2006), which impede bar formation and thus channel shift.

Copyright © 2015 John Wiley & Sons, Ltd.

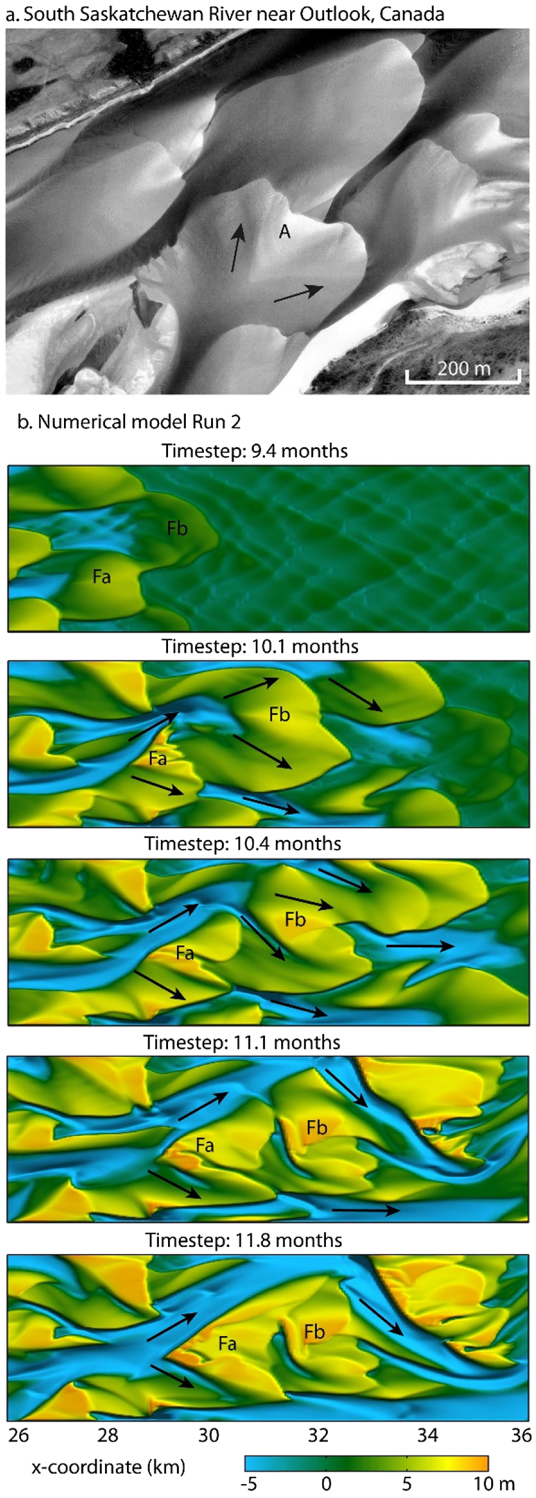

Figure 4. Examples of conversion of unit bars into compound bars in (a) South Saskatchewan River and (b) run 2 for bar F (see Figure 3). Aggradation of unit bars results in flow bifurcation around the bar centre, each branch forming its own unit bar and bar-tail limb, e.g. bars Sa, Sb, Sd, Fa and Fb. Note the similarity in bar shape between bar Sa in the South Saskatchewan River and bar Fb in the model after 10.1 months. After the conversion, downstream expansion of bar Fa resulted in agglomeration of bars Fa and Fb (bifurcation closure mechanism 7 in Figure 9). Aerial photo courtesy of Sambrook Smith, Ashworth, Best and Lane. This figure is available in colour online at wileyonlinelibrary.com/journal/espl

Bifurcation evolution mechanisms

Multiple mechanisms for bifurcation initiation could be recognized in the self-formed braided river in addition to the conversion of unit bar into compound bars. One mechanism was the chute cutoff: a bank-attached bar that was disconnected from the outer banks and thus became a mid-channel bar. An example is given in Figure 7, in which bar G was bank-attached until month 16. A similar mechanism was cross-bar flow initiating a cross-bar channel and dissecting the bar (Figure 8). The contribution of each bifurcation initiation mechanism depended on the evolution stage of the river (Figure 9): initiation of unit bars dominated at the front of the bars induced by upstream discharge perturbation, whereas bar dissection by cross-bar channelization dominated in the mature stage of the river. However, the different bifurcation closure mechanisms are equally important. Closure of bifurcation branches by bar expansion and merging of branches due to widening of one of the branches are, however, the more important mechanisms in the mature stage of the river. Closure of branches by bar expansion was often caused by bar-tail limbs, as the relatively low bar-tail limbs expanded faster than upstream erosion of the next bar. Almost all compound bars had two, and sometimes more, bar-tail limbs.

Locally, transverse water-level differences between parallel channels due to differences in flow depth and resistance, and causing over-bar flow, played a key role in chute cutoffs and cross-bar channelization. For example, the chute cutoff in Figure 7 was caused by a water-level depression in the lee side of bar G (Figure 7c). The water-level depression was the result of closure of the upstream supply branch between bars G and H, and thus isolation of the area. The water-level depression attracted flow, and this resulted in a chute cutoff at the most upstream location, where the water-level difference was at the maximum. Also, examples of cross-bar flow induced by water-level impoundment were found, for example upstream of the bar at x = 53 km (Figure 8). In this case, bar expansion narrowed the discharging branch, resulting in a backwater effect, water-level impoundment and cross-bar flow.

Bar expansion, bar merging and finally bar dissection occurred as a continuous cycle, for example in Figure 10. In this example, the bar-tail limb of compound bar A expanded and merged with bar B in month 22. This resulted in a water-level depression in the north of bar A+B and eventually formed a cross-bar channel, disconnecting bar A from B in months 25–28. Because the majority of discharge went through the channel south of bars A and B, the bar-tail limb of bar A elongated in downstream direction between months 34 and 37. Eventually, the elongated bar-tail limb reconnected bars A and B and closed one cycle.

Application of nodal point relations

The nodal point relations for predictions of discharge and sediment division were tested for two bifurcations at bars C and F (Figure 5). The evolution of the bifurcation of bar C differed from bar F: bar C started with an almost symmetric bifurcation (Figure 11 and Figure 12) and evolved into a bank-attached bar due to closure of the northern branch 4 (Figure 11a). Bar F started with an asymmetric bifurcation (3:2 ratio of water and sediment discharge) and evolved into a more asymmetric bifurcation (Figure 11 and Figure 12).

The discharge division predicted by the nodal point relations correlates poorly with the 'real' discharge division in the three-dimensional model (Figure 13a, b). The discharge division predicted by the channel width ratio fitted better than using the Chezy equation. Although the order of magnitude is correct, neither of the two nodal point relations recover the trends of discharge division computed with the three-dimensional model. This indicates that the effects of

Copyright © 2015 John Wiley & Sons, Ltd.

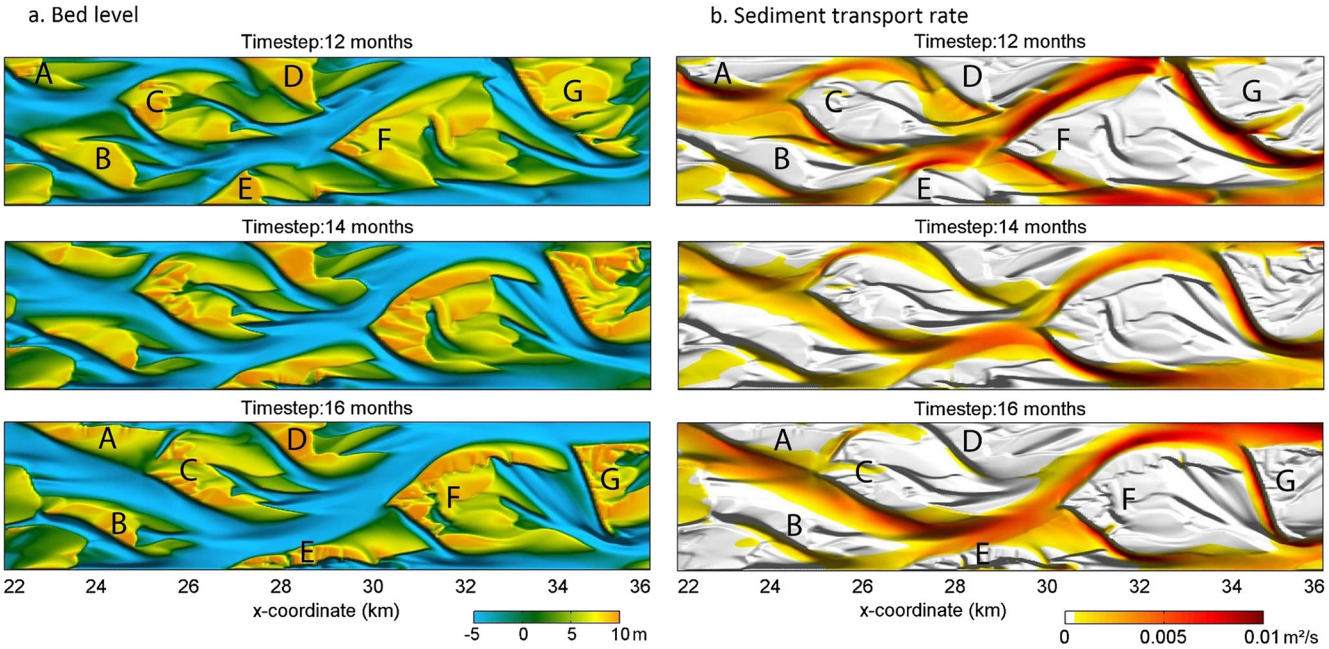

Figure 5. Evolution of two bifurcations upstream of bars C and F in run 2. The branch between bars A and C closed due to downstream expansion of bar A. Thus bar C becomes a bank-attached bar. At the same time, the bifurcation of bar F becomes more asymmetrical. This could be due to a change in bifurcation angle and flow direction of the channel in the north of bar E. This figure is available in colour online at wileyonlinelibrary.com/journal/espl

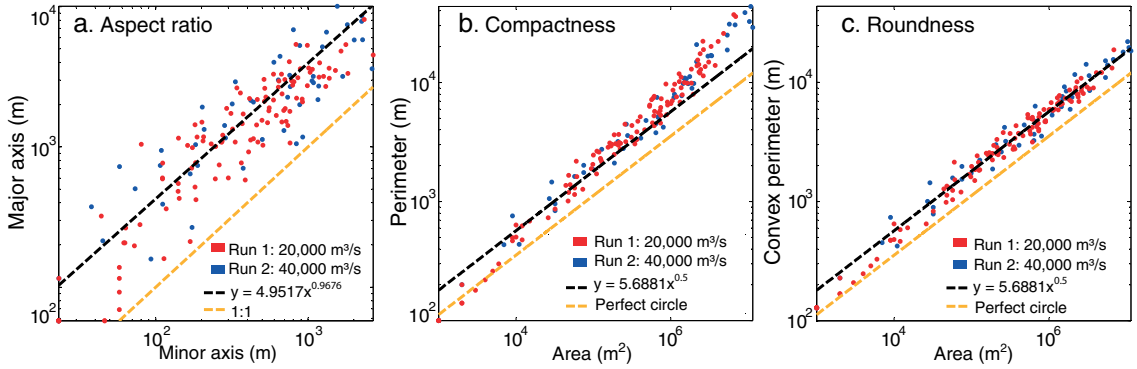

Figure 6. Bar shapes in run 1 (after 34 months, see Figure A of the online supplementary material), and run 2 (after 15 months,): (a) aspect ratio; (b) compactness; (c) roundness. Empirical relations of Kelly (2006) were added for comparison with natural rivers. Note the difference between b and c for the larger bars, showing that large bars have more complicated and irregular shape than small bars. This figure is available in colour online at wileyonlinelibrary.com/journal/espl

non-uniformity, or 'three-dimensionality', of the flow dominate the signal.

Predictions of sediment division using the nodal point relations are even less accurate (Figure 13c, d), regardless of the discharge distribution data source. Apparently, the simplification made by Wang *et al.* (1995) to relate sediment division only to channel widths, discharge division and an empirical parameter k is inaccurate, or at least not captured by one-dimensional data or branch-averaged data. Also, the assumption of Bolla Pittaluga *et al.* (2003) that sediment division is only based on channel widths and transverse sediment transport at the node is inaccurate in this context. The recorded ratios of bars C and F showed a similar pattern of decrease in sediment transport ratio $Q_{s3,6}/Q_{s4,5}$ without a significant change in discharge ratio $Q_{3,6}/Q_{4,5}$ (Figure 13c–f). After that, $Q_{s3,6}/Q_{s4,5}$ increased and were accompanied by a gentle increase in $Q_{3,6}/Q_{4,5}$. These patterns were captured neither by the one-dimensional models for sediment transport division nor by the different discharge division predictors. These results will be discussed later.

To predict bifurcation evolution, it is necessary to combine predicted discharge divisions and sediment divisions, using predicted discharge divisions as input for the sediment division predictors. In accordance with the individual predictions of discharge and sediment division, Figure 13 shows little similarity between the predicted ratios from the nodal point relations and ratios from the three-dimensional mode (Figure 13c–f).

We identified multiple reasons for the instability of the bifurcations of bars C and F that are not accounted for in the nodal point relations. In both cases, an upstream bar (bars A and E) expanded and, consequently, the entrance of one of the branches was narrowed. This downstream expansion of bars A and E means that sediment transport rates in the branches declined downstream of the bifurcation. An important forcing condition was the evolution of channel 2 upstream of bar C (Figure 3). This channel gave flow directions that favoured the southern channel 3 around bar C, because of a small angle towards the southern branch compared to towards the northern branch. As branch 4 closed, most of the discharge flowed

Copyright © 2015 John Wiley & Sons, Ltd.

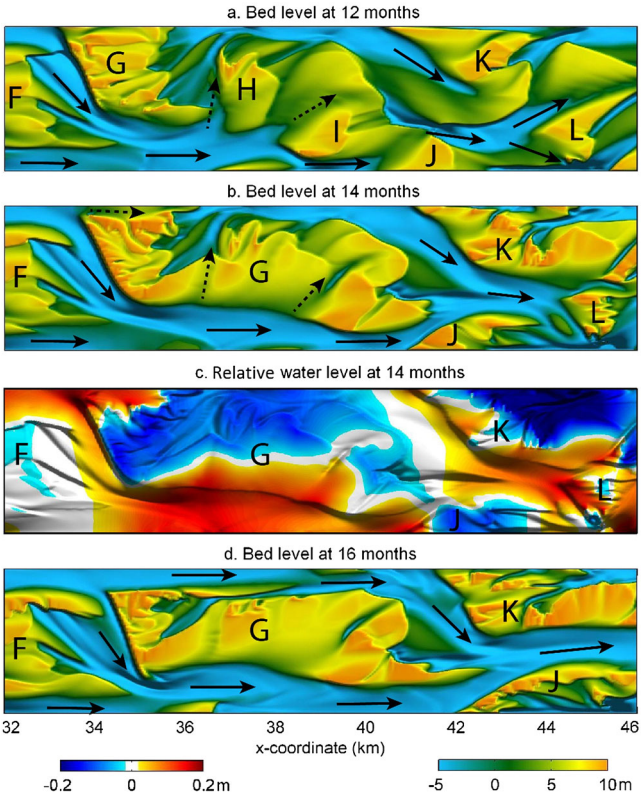

Figure 7. Evolution of a bank-attached bar into a mid-channel bar in run 2 by bifurcation initiation mechanism 4 (see Figure 9). Expansion of bars G and H resulted in merging of bars G, H and I after 14 months (b). This large bar blocked discharge to the channel in the north of bar G, resulting in a lateral water slope between the northern and southern channel around bar G (c). This lateral water slope induced an increase of flow along the banks in the north of bar G, ultimately resulting in a chute cutoff and the release of bar G from the banks (d). Solid arrows indicate dominant flow direction; dotted arrows indicate minor flow direction. This figure is available in colour online at wileyonlinelibrary.com/journal/espl

through channel 3. As a result, the bifurcation angle towards the bifurcation of bar F favoured discharge towards branch 6.

Application of planform-based predictors

An alternative predictor for near-future bifurcation evolution is the planform shape of the bifurcation itself and the shape of nearby bars and channels. Length, width and shape of bar-tail limbs are clearly indicators of the prevailing flow direction (Figures 5 and 14), in agreement with Koomen (1992), Ashworth *et al.* (2000) and Schuurman *et al.* (2013). Bar-tail limb elongation occurred when the flow was parallel to the bar-tail limb, indicating prevailing flow to the opposite bifurcation branch. Lateral bar-tail limb expansion occurred when the flow was normal to the bar-tail limb, by deposition of sediment in the lee zone of the bar-tail limb. Thus a bar-tail limb only closed a bifurcation branch if it was not the dominant branch. An example of this is given in Figure 10, which shows that the bar-tail limb of bar A expanded in a downstream direction, growing into the branch between bars A and B. In contrast, the bar-tail limb at the south of bar B did not grow into its adjacent branch, or only during a short period (months 25–28) when the cross-bar channel was formed and thus attracted discharge.

Another planform-based indicator is the bifurcation angle asymmetry. The deviation angle of the minor branch to the inflow channel direction was often higher than that of the dominant branch and increased with time (Figure 10). This increase of deviation angle was coupled with expansion of the upstream bar-tail limb of bar A and erosion of the upstream part of bar B. The same pattern occurred in run 2 (Figure 7). While bars A and E expanded into the adjacent branches, the bar-tail limbs of bars C and D curved parallel to the dominant northern channel but did not expand. As shown in Figure 15, the bifurcation angle asymmetry correlated well with discharge division and the water-level difference between the parallel branches. These results show that bifurcation angle asymmetry indicates the dominant branch and the degree of closure of the minor branch. In contrast, there was no clear relation between sediment division and bifurcation angle asymmetry (Figure 15). The reason for this is the three-dimensionality of the morphodynamics, in particular the migration of bars into the bifurcation that affects the sediment transport rates.

Discussion

Initiation and evolution of mid-channel bars and bifurcations

Unit bar initiation is caused by non-uniformity of sediment transport rate due to initial bed perturbation and upstream inflow perturbation. These unit bars evolve into compound bars as they aggrade, each initiating a bifurcation. This process is also common in flume experiments (e.g. Ashmore, 1991; Ferguson, 1993; Ashworth, 1996) and observed in nature (e.g. Rozo *et al.*, 2012). Unit bar conversion is the dominant bifurcation initiation mechanism in the early stage of the river evolution, when bars are low compared to the water depth. This is comparable to the observations of Wheaton *et al.* (2013), who showed that unit bar conversion is more important during periods with high water levels.

At a later stage, when the maturing bars reach the water surface, bifurcation initiation proceeds from bar splitting. We see two styles of bar splitting: the classic chute cutoff, which has a general downstream direction, and cross-bar flow leading to cross-bar channels. When such cross-bar channels enlarge they may also become more aligned with the general flow direction and resemble the chute channels. The

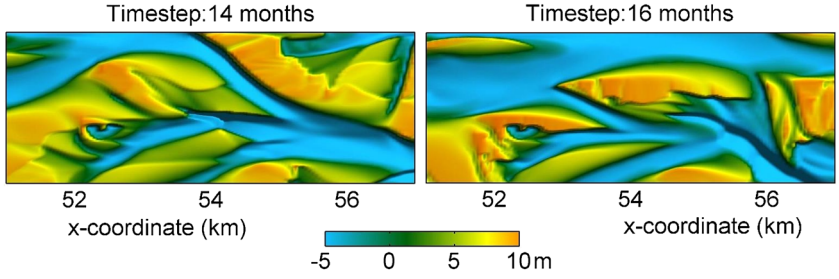

Figure 8. Example of bifurcation initiation mechanism 6 (see Figure 9) in run 2: dissection of a large mid-channel bar by over-bar flow, resulting in a new mid-channel bar and consequently a new bifurcation. This figure is available in colour online at wileyonlinelibrary.com/journal/espl

Copyright © 2015 John Wiley & Sons, Ltd.

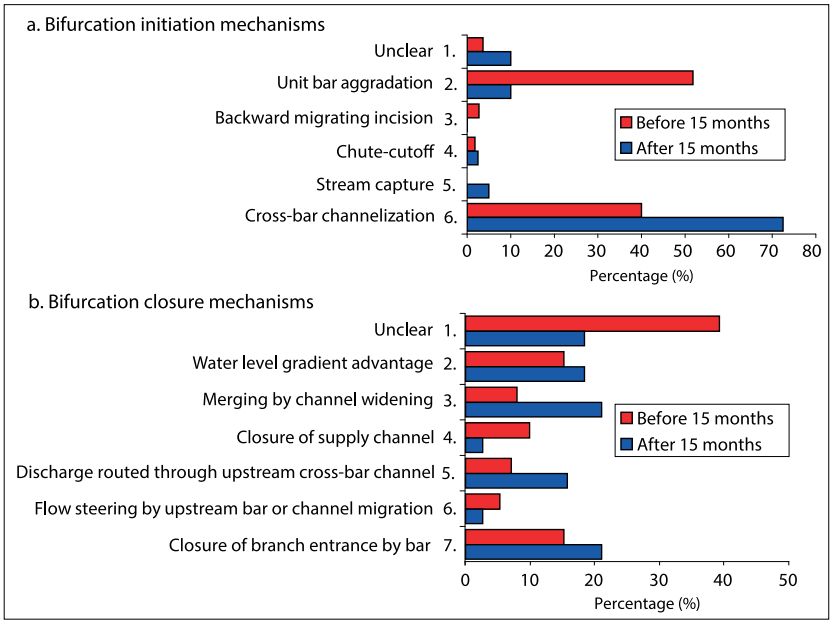

Figure 9. Relative occurrence of bifurcation initiation and closure mechanisms in run 2. This figure is available in colour online at wileyonlinelibrary.com/journal/espl

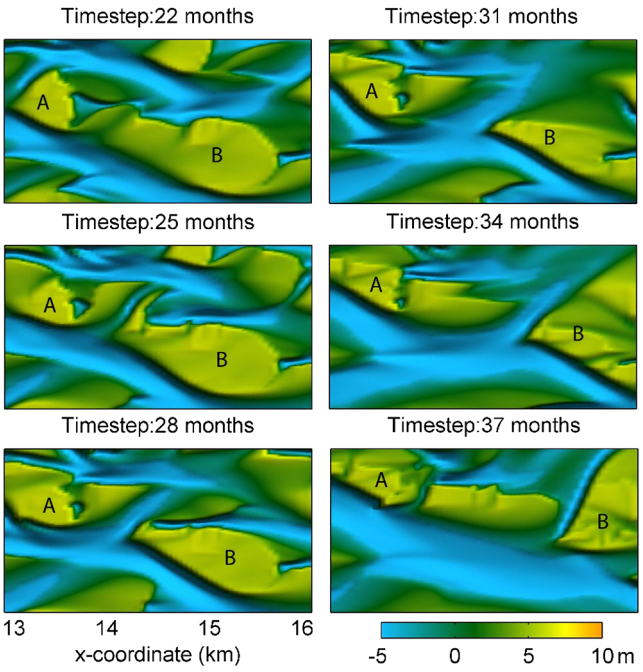

Figure 10. Cycle of a bifurcation initiation and closure in run 1. Bars A and B are attached by a bar-tail limb of bar A. This results in a water-level depression in the north of bar B, which initiates a cross-bar channel and separation of both bars. Later, a bar-tail limb of bar A expands parallel to the dominant flow direction, closing the entrance of the northern branch around bar B. This figure is available in colour online at wileyonlinelibrary.com/journal/espl

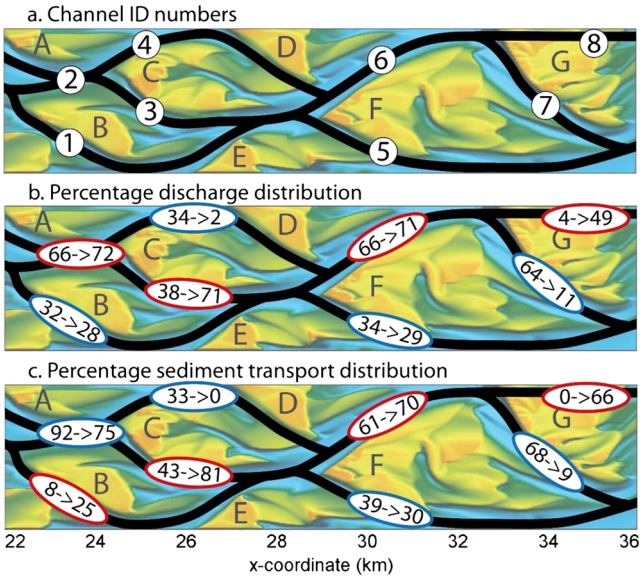

Figure 11. ID numbers of the branches in the simulated river run 2 (a); discharge division as a percentage of the cross-sectional total discharge (b); sediment transport division as a percentage of the cross-sectional total sediment transport (c). The first number in each ellipse of b and c shows the simulated divisions after 12 months; the second value is after 17 months; red ellipses indicate an increase; blue ellipses indicate a decrease. This figure is available in colour online at wileyonlinelibrary.com/journal/espl

cross-bar channel formation was also observed in low-flow conditions in a braided gravel-bed river by Wheaton *et al.* (2013). A similar phenomenon has been observed in estuaries, where tidal phase differences between channels flanking a tidal bar set up a gradient over the bar that leads to channel incision (Van den Berg *et al.*, 1996; Swinkels *et al.*, 2009). These works indicate that this mechanism for channel incision through bars in multichannel systems generally occurs in various environments.

Our modelled river showed no clearly dominating bifurcation closure mechanism. The consequence of bifurcation closure is merging and expansion of compound bars, as also often observed in nature (e.g. Ashworth *et al.*, 2000, 2011; Lunt *et al.*, 2004; Best *et al.*, 2003; Mumpy *et al.*, 2007). In turn, the expansion of bars and their attachment to the banks of the braidplain result in (partial) blockage of discharge through the channel branch and, consequently, the impoundment of local water level. This causes a lateral water surface slope between the two sides of a mid-channel bar, providing a potential for cross-bar flow and ultimately bar dissection, as often observed in nature (e.g. Figure 1a). When planform equilibrium is statistically defined by a distribution of bar

Copyright © 2015 John Wiley & Sons, Ltd.

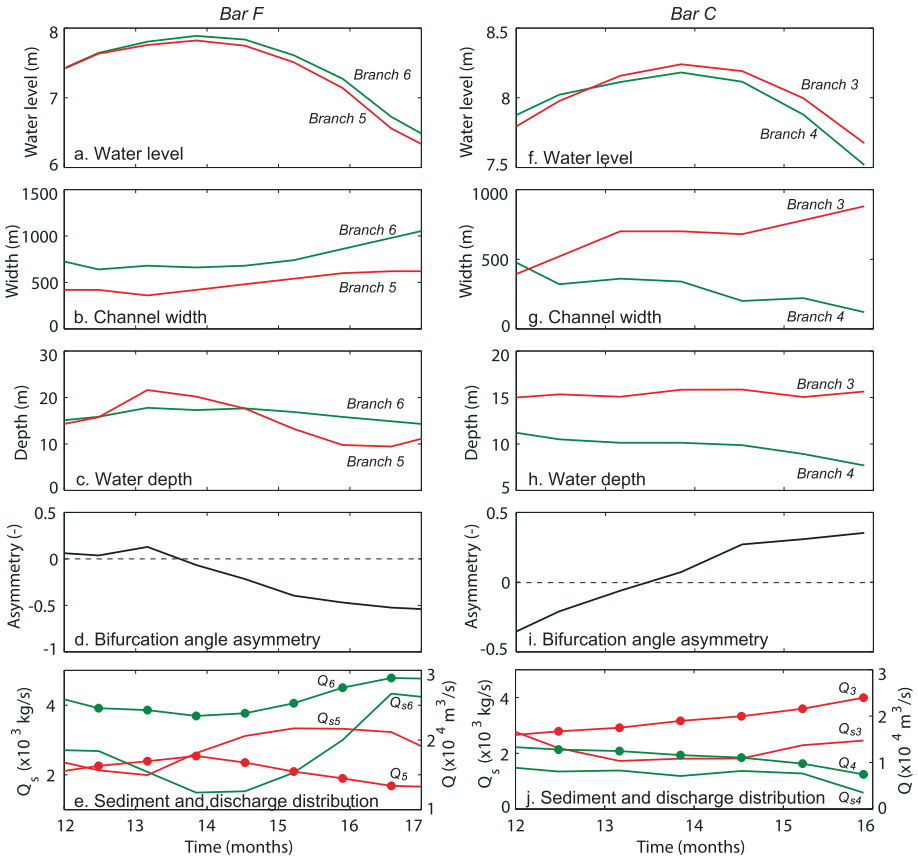

Figure 12. Bifurcation properties and sediment and discharge divisions over the bifurcation of bar F (left) and bar C (right) in Figures 5 and 11 of run 2. This figure is available in colour online at wileyonlinelibrary.com/journal/espl

dimensions, the frequency of bifurcation creation by bar dissection balances the frequency of bifurcation closure, which leads to bar merging.

The larger compound bars in the self-formed river were relatively stable, and immobilized neighbouring smaller bars and channels. So, even though we used the least amount of topographic forcing by applying an initially flat bed and uniform channel width, the self-formed river developed its own topographic forcing. This reduced the overall dynamics, limiting morphodynamics to the bar edges and shallow bar-tail limbs. The lack of a physics-based bank erosion module in the model and the fixed braidplain banks induced incision of the channels, as also found in flume (Ashworth *et al.*, 2000) and nature (Mosselman, 2006). This resulted in relatively deep channels with limited new bar formation.

Despite the simplified conditions, constant boundary conditions and simplification or absence of certain processes, for example the straight braidplain with non-erodible banks, constant discharge, and ignorance of vegetation, grain size variation and cohesive sediment, the numerical model produced many realistic aspects of a natural braided river. This suggests that if these factors are to be included an even higher degree of realism in a self-formed topography could be achieved (Nicholas, 2013a, 2013b). Nevertheless, significant improvement of rules for vegetation dispersal, growth and mortality is necessary to realistically model the interaction between vegetation, hydrodynamics and morphodynamics.

The model simulations demonstrated the importance of network connectivity for bar, branch and bifurcation evolution, in agreement with Marra *et al.* (2013). For example, the water-level impoundments or depressions after bar merging shown in Figure 7 had a wide influence zone, as it affected upstream bifurcations by favouring discharge towards the depressions and favouring over-bar flow. Also, discharge through the branches affected lateral shifting of branches, as discharge increase and higher flow velocities stimulate branch shift and thus merging of branches and rotating of approaching flow towards downstream bifurcations. Indeed, most of the bifurcation closure mechanisms identified in the simulations are caused by changes in upstream bifurcations.

Prediction methods for short-term bifurcation, bar and channel evolution

Our simulations, and multiple field observations and flume experiments, showed a complicated relation between bifurcation evolution and bar dynamics. The concept of discharge and sediment division determining deposition and incision that has been used in the nodal point relations appeared to be an oversimplification, in agreement with Zolezzi *et al.* (2006). This is explained by three-dimensional effects and processes at the bar scale and at the reach scale, such as non-uniformity in the branches (Figure 16c, e), inflow steering by local topography (Figure 16b), inflow channel shift (Figure 16d), backwater effects (Figure 16e) and other changes in the network that propagate to a bifurcation of interest. Thus the nodal point relations appear to have limited predictive value for bifurcation evolution in braided rivers in which local three-dimensional effects and reach-scale network effects dominate. However, nodal point relations remain useful for perturbation analyses that seek to investigate causes of instability of bifurcations (Bolla Pittaluga *et al.*, 2003) and for modelling single-thread rivers and rivers with fixed banks (Kleinhans *et al.*, 2011).

On the other hand, two planform-based indicators were found to qualitatively predict near-future bifurcation evolution: presence, position and size of bar-tail limbs, and bifurca-

Copyright © 2015 John Wiley & Sons, Ltd.

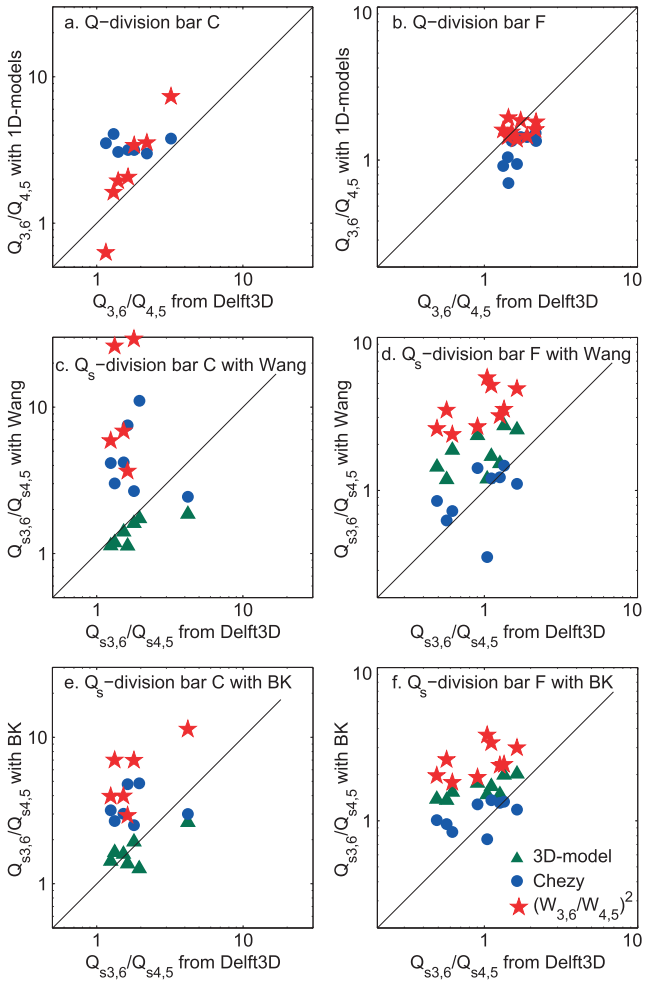

Figure 13. Comparison of discharge division (Q in a, b) and sediment division (Q_s in c, d) for bars C (left) and F (right) between the 3D model and the nodal point relations. For the sediment division prediction we used the two nodal point relations and the flow observed in the 3D model. The black lines indicate $y = x$. This figure is available in colour online at wileyonlinelibrary.com/journal/espl

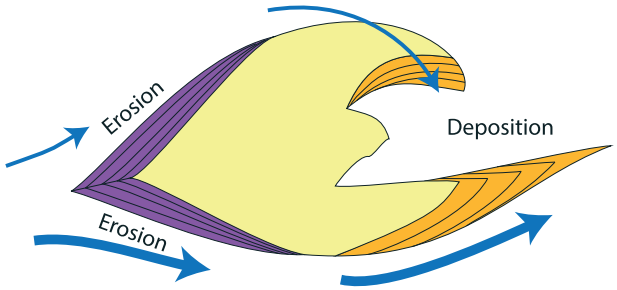

Figure 14. Concept of how evolution of bar-tail limbs depends on the dominance of the bifurcation branch. Elongation occurs parallel to the main flow in the dominant branch, whereas the bar-tail limb in the recessive branch remains short. The bar-tail limb widens when flow occurs from the recessive branch towards the dominant branch, e.g. because of downstream closure of the recessive branch. This figure is available in colour online at wileyonlinelibrary.com/journal/espl

tion angle asymmetry or deviation angle. In several examples, dominant bifurcation branches and prevailing flow directions correlated with the length and width of bar-tail limbs, in agreement with Ashworth *et al.* (2000) and Best *et al.* (2003). Bifurcation angle asymmetry is an indicator of discharge division and of the likelihood of entrance closure by a migrating or expanding bar, agreeing with Koomen (1992) and Best *et al.* (2008). The bar-tail limb is an indicator for erosion of the bar flank at that side of the bifurcation. Thus, when a particular bifurcation asymmetry is conducive to channel growth, this also causes enhanced bank erosion at the bifurcation, which supplies extra sediment to the enlarging channel. Potentially, this extra sediment supply acts as a negative feedback as it narrows the channel and reduces the sediment transport capacity. The sediment is deposited in a bar-tail limb, of which the dimensions and growth rate are an indicator of the rate of bifurcation erosion and upstream channel growth. But there is also a downstream influence of the channel network, in particular the next bifurcation: the expanding bar-tail limb curves with the main flow direction downstream of the bar towards the dominant downstream branch. These connections between the development and the observable planform geometry are potentially useful in practice as the required observations can easily be extracted from aerial photos and/or satellite images with sufficient detail, which is valuable in areas where measurements are lacking.

Both the use of bar-tail limbs and of bifurcation angle as indicators for near-future bifurcation evolution need further investigation, considering that discharge variation and deposition of fines in the protected area between the bar-tail limbs might affect the shape and growth of bar-tail limbs and bifurcations. We attempted to correlate bar-tail limb volume changes to changes of bifurcation planform by segmentation of all individual bars and division of the bars in quadrants. However, the compound bars are so irregular and asymmetrical that this relatively straightforward method of automated pattern recognition failed to recognize bar-tails and capture the trends that the human eye can detect in images.

We propose a conceptual model to aid inference of the evolution of the channel network from the development of bar-tail limbs and bifurcation planform from imagery. The conceptual model is based on the evolution cycle of interacting bars, channels and bifurcations, caused by local water-level

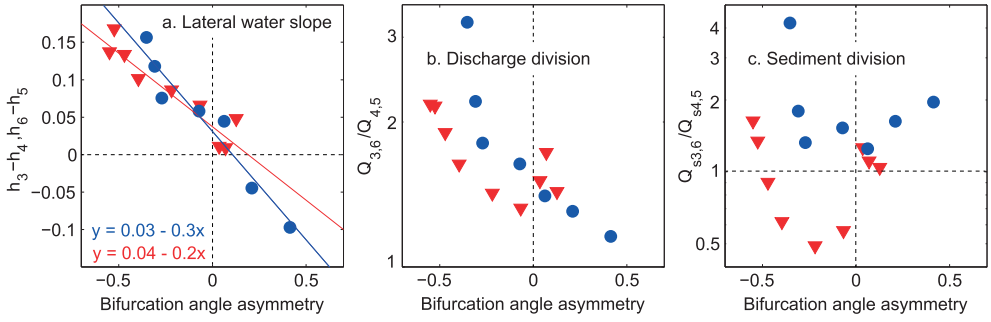

Figure 15. Relations between later water-level difference and bifurcation angles (a), discharge divisions (b) and sediment divisions (c) for bars C (blue circles) and F (red triangles). Bifurcation angle asymmetry is defined as $(a3 - a4, a6 - a5)/a1$ (see Figure 2). This figure is available in colour online at wileyonlinelibrary.com/journal/espl

Copyright © 2015 John Wiley & Sons, Ltd.

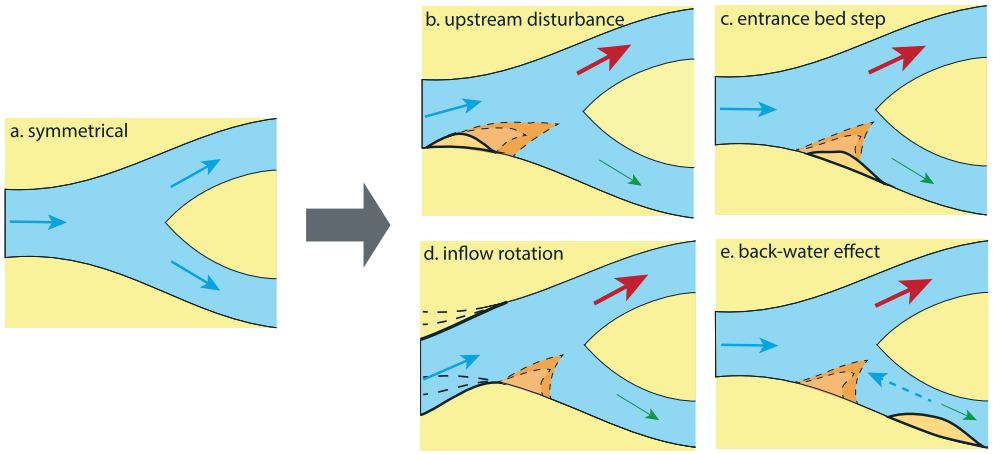

Figure 16. Evolution of a symmetrical bifurcation (a) into an asymmetrical bifurcation in response to migration of an upstream bar (b), an inlet step or bar at the entrance of one of the downstream branches (c), changing direction of upstream flow (d) or a backwater effect due to a downstream bar (e). In all cases a bar-tail limb develops. This figure is available in colour online at wileyonlinelibrary.com/journal/espl

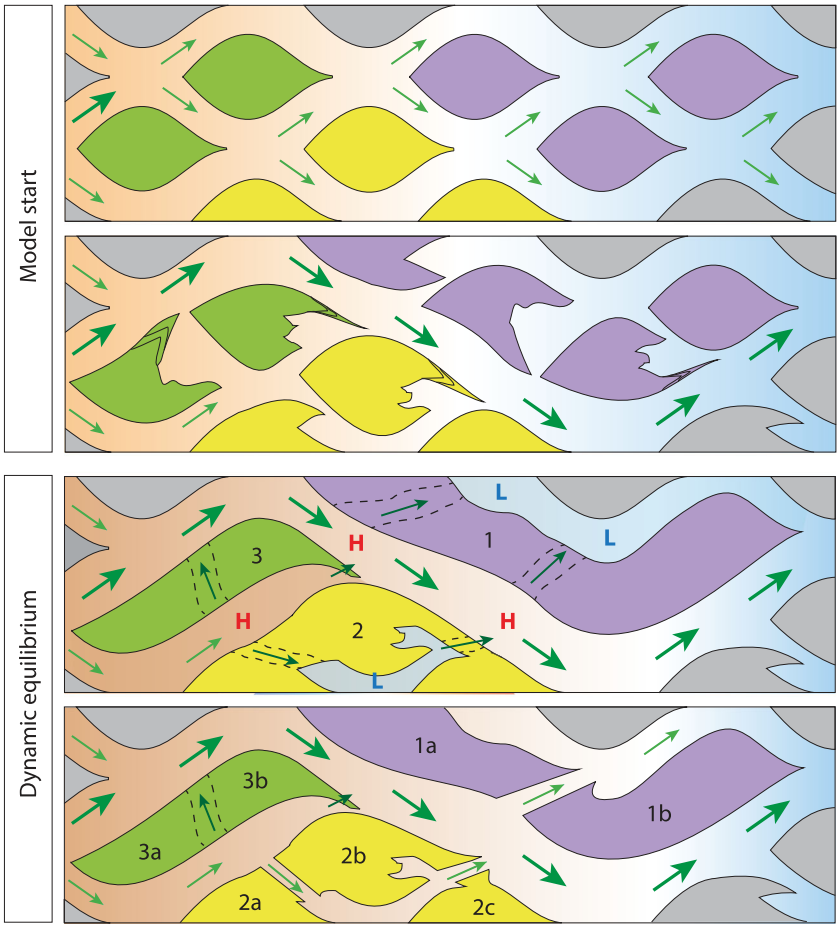

Figure 17. A cycle of bar evolution in a braided river: bar initiation, growth of bar-tail limbs parallel to the prevailing flow, bar merging by closure of bifurcation branches, and bar dissection by cross-bar flow. Connected bar groups have distinct colours for clarity. Note different high-water colours in parallel branches indicating high water level (red, H) and low-water level (blue, L) relative to average water level. This figure is available in colour online at wileyonlinelibrary.com/journal/espl

non-uniformities, typical evolution of mid-channel bars often with bar-tail limbs (Figure 14) and typical disturbances in bifurcations (Figure 16). The model simulations showed a cycle of (i) bar expansion by deposition of shallow bar-tail limbs; (ii) bar merging by bar-tail limbs connecting adjacent bars; (iii) disconnection and local narrowing of channel branches causing lateral water level non-uniformity; and (iv) initiation of new branches by cross-bar flow; and ultimately bar dissection, which results in smaller bars. We identified three main causes for water-level non-uniformities (Figure 17). First, an upstream closure of a branch causes a water-level depression in the disconnecting channel (Figure 17, bar 1). This can induce cross-bar flow from the main channel towards the disconnected branch and splitting of bar 1. Second, downstream closure causes upstream impoundment (between bars 2 and 3) and asymmetry of the upstream bifurcation (of bar 3). Third,

Copyright © 2015 John Wiley & Sons, Ltd.

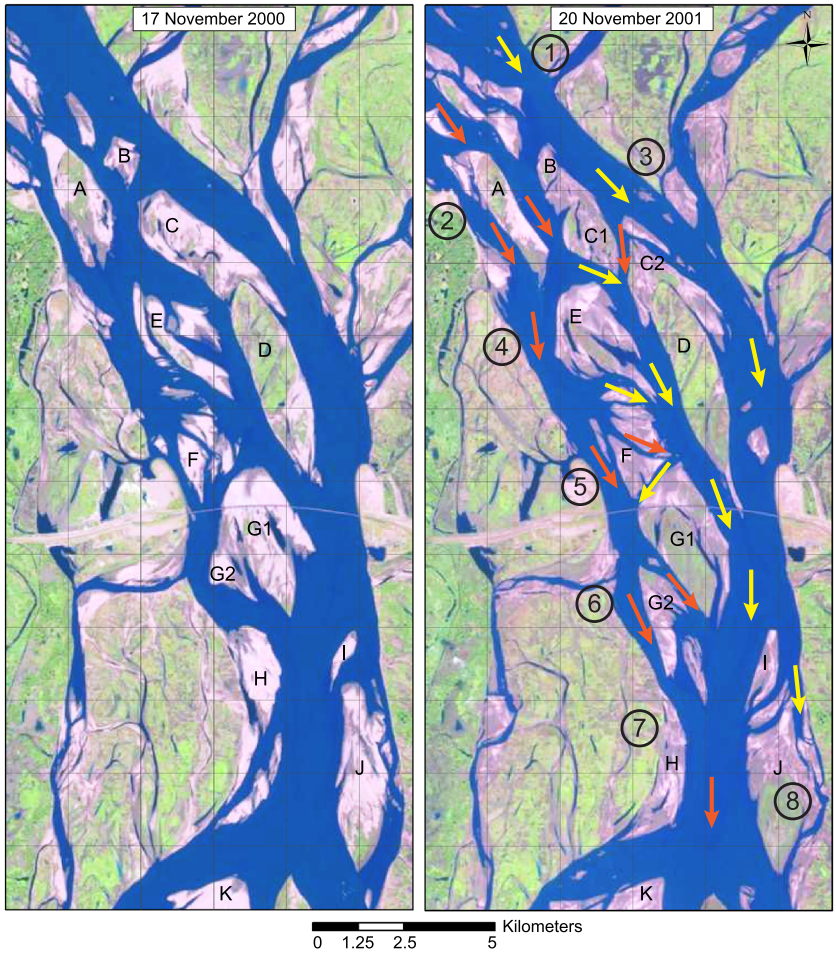

Figure 18. Example of interacting dynamics of bars, islands, bifurcations and branches in the Brahmaputra River (Bangladesh) between 17 November 2000 and 20 November 2001. Prevailing flow directions in the branches are indicated by arrows: red arrows for increasing branch discharge; yellow arrows for decreasing branch discharges. Numbers and bar names are referred to in the text. Source: Landsat 7 Satellite image (http://earthexplorer.usgs.gov). This figure is available in colour online at wileyonlinelibrary.com/journal/espl

a combination of upstream and downstream disconnection results in an isolated water body that is relatively easy to reuse after a chute cutoff (bar 2).

We applied the conceptual model to a 25 km section of the Brahmaputra River in Bangladesh, near the Jamuna Bridge (Figure 18). Based on our conceptual models, we suggest the following explanation for the morphodynamics, where the numbers refer to the numbers on the map of 2001:

1. Upstream flow shifted from the east towards the west, which we now regard as boundary condition.
2. Increased discharge around bar A caused expansion of bar A in the prevailing flow direction (SE) and erosion of its flanks.
3. Also, bar B expanded, closing the branch between bar B and C1. A new cross-bar channel formed between bars C1 and C2, causing, among others, the formation of bar-tail limbs draped around the stable bar D.
4. The alteration of bars A, B and C changed the approaching flow for the bifurcation of bar E, causing discharge increase towards the western branch.
5. This changed the approaching flow intensity and direction of the bifurcations of bars F and G1, resulting in widening of the western branch along bar F. The eroded sediment deposited at the downstream lee of bar F, narrowing the branch between bar F and G1.
6. The discharge increase in the west branch along bar F increased discharge between bars G1 and G2, causing bar dissection. As the chute channel was not fully developed, the western bar-tail limb of bar G2 could still elongate. At the same time, the bar-tail limb along the east-side of bar G1 expanded in downstream direction and curved with prevailing flow.
7. The discharge increase of the western branch of bar G2 resulted in downstream migration of bar H, providing space for elongation of the bar-tail limb of bar G2.

This example shows the network aspect in the braided river section, and a way to interpret the network planform, including bifurcation angles and changes in bar-tail limb lengths and directions. This study shows that bifurcation evolution is affected by the evolution of adjacent bifurcations and bars, thus being part of a chain-like network of interacting bifurcations and bars. Further development of the spatial and temporal linkages between channels and bars is required and has potential application in large braided rivers with high population pressure where efficient dredging strategies and sustainable flood and bank protection measures are needed.

Conclusions

We investigated initiation and evolution of bifurcations and bars in the channel network of a large braided sand-bed river. Based on our simulations and analyses, we conclude the following:

1. In the early stage starting from plane bed, mid-channel bars and bifurcations are formed mainly by transverse bar dissection, when unit bars evolve into compound bars. Bars

Copyright © 2015 John Wiley & Sons, Ltd.

force the initiation of bars further downstream, resulting in a downstream migration of a front of unit bars. The evolution of a unit bar into a compound bar occurs by aggradation on the bar, steering the main flow around the bar centre, inducing channelization, isolation of the bar centre and downstream deposition on bar-tail limbs.

2. In a fully developed braided river, a cycle of bar expansion, bar merging and bar dissection occurs. Bifurcations are most frequently initiated by cross-bar channelization, caused by water-level differences between branches separated by a bar. Modelling this process requires a high grid resolution. Although no mechanism for bifurcation closure dominates, bar-tail limb expansion and bar merging often close off bifurcations.
3. Bar expansion and migration, especially the development of bar-tail limbs, and channel migration affect bifurcation evolution. These morphodynamic processes only partly emerge in the nodal point relations, that also neglect non-uniform flow conditions within the branches, flow steering by channel curvature and bars, and over-bar flow. This means that nodal point relations for predicting discharge and sediment division, though successful in other environments, are of limited value for braided sand-bed rivers.
4. On the other hand, bar-tail limbs and bifurcation angle asymmetry are observable indicators with predictive value for asymmetry and evolution of a bifurcation: bar-tail limbs indicate dominant bifurcation branches and dominant flow direction, whereas a large-angle asymmetry of a bifurcation points at the closing branch. The proposed conceptual model was successfully tested on consecutive satellite images of a large river.

Acknowledgements— MGK and FS are supported by the Netherlands Organization for Scientific Research (NWO) (grant ALW-Vidi-864-08-007 to MGK). We gratefully acknowledge the visual classification of the river bifurcation development by Eveline van der Deijl. We thank Hans Middelkoop, Erik Mosselman, Wouter Marra and Tjalling de Haas en Trang Vu for discussion and comments on the manuscript. The aerial photo in Figure 4 was produced as part of NERC grant NER/A/S/2003/00538 awarded to Sambrook Smith, Ashworth, Best and Lane. Deltares and Royal HaskoningDHV are acknowledged for collaboration. The authors contributed in the following proportions to conception and design, modelling, analysis and conclusions, and manuscript preparation, respectively: FS(60%, 100%, 80%, 90%), MGK(40%, 0%, 20%, 10%).

References

Ashmore PE. 1991. How do gravel-bed rivers braid? *Canadian Journal of Earth Sciences* **28**(3): 326–341.

Ashworth JP. 1996. Mid-channel bar growth and its relationship to local flow strength and direction. *Earth Surface Processes and Landforms* **21**(2): 103–123.

Ashworth JP, Best JL, Roden JE, Bristow CS, Klaassen GJ. 2000. Morphological evolution and dynamics of a large, sand braid-bar, Jamuna River, Bangladesh. *Sedimentology* **47**(3): 533–555.

Ashworth JP, Sambrook Smith GH, Best JL, Bridge JS, Lane SN, Lunt IA, Reesink AJH, Simpson CJ, Thomas RE. 2011. Evolution and sedimentology of a channel fill in the sandy braided South Saskatchewan River and its comparison to the deposits of an adjacent compound bar. *Sedimentology* **58**(7): 1860–1883.

Bertoldi W. 2012. Life of a bifurcation in a gravel-bed braided river. *Earth Surface Processes and Landforms* **37**(12): 1327–1336.

Bertoldi W, Tubino M. 2005. Bed and bank evolution of bifurcating channels. *Water Resources Research* **41**. DOI:10.1029/2004WR003333.

Bertoldi W, Zanoni L, Tubino M. 2009. Planform dynamics of braided streams. *Earth Surface Processes and Landforms* **34**(4): 547–557.

Best JL, Ashworth JP, Bristow CS, Roden JE. 2003. Three-dimensional sedimentary architecture of a large, mid-channel sand braid bar, Jamuna River, Bangladesh. *Journal of Sedimentary Research* **73**(4): 516–530.

Best JL, Woodward J, Ashworth JP, Sambrook Smith GH, Simpson CJ. 2006. Bar-top hollows: a new element in the architecture of sandy braided rivers. *Sedimentary Geology* **190**(1–4): 241–255.

Best JL, Ashworth PJ, Sarker MH, Roden JE. 2008. The Brahmaputra-Jamuna River, Bangladesh. In *Large Rivers: Geomorphology and Management*, Gupta A (ed), Wiley: Chichester; 395–433.

Bolla Pittaluga M, Repetto R, Tubino M. 2003. Channel bifurcation in braided rivers: equilibrium configurations and stability. *Water Resources Research* **39**(3): 1046.

Bridge JS. 1993. The interaction between channel geometry, water flow, sediment transport and deposition in braided rivers. In *Braided Rivers*, Best JL, Bristow CS (eds), Geological Society: London; 13–71.

Bristow CS. 1993. Sedimentary structures exposed in bar tops in the Brahmaputra River, Bangladesh. In *Braided Rivers*, Best JL, Bristow CS (eds), Geological Society: London; 277–289.

Crosato A, Mosselman E. 2009. Simple physics-based predictor for the number of river bars and the transition between meandering and braiding. *Water Resources Research* **45**. DOI: 10.1029/2008WR007242.

Deltares. 2009. *Delft3D-FLOW.* User manual: simulation of multi-dimensional hydrodynamic flows and transport phenomena, including sediments. Deltares: Delft.

Egozi R, Ashmore P. 2008. Defining and measuring braiding intensity. *Earth Surface Processes and Landforms* **33**(14): 2121–2138.

Engelund F, Hansen E. 1967. *A Monograph on Sediment Transport in Alluvial Streams*. Danish Technical Press: Copenhagen.

Federici B, Paola C. 2003. Dynamics of channel bifurcations in noncohesive sediments. *Water Resources Research* **39**(6). DOI:10.1029/2002WR001434.

Federici B, Seminara G. 2003. On the convective nature of bar instability. *Journal of Fluid Mechanics* **487**: 125–145.

Ferguson RI. 1993. Understanding braiding processes in gravel-bed rivers: progress and unsolved problems. In *Braided Rivers*, Best JL, Bristow CS (eds), Geological Society: London; 73–87.

Kelly S. 2006. Scaling and hierarchy in braided rivers and their deposits: examples and implications for reservoir modeling. In *Braided Rivers: Process, Deposition, Ecology and Management*, Smith GHS, Best JL, Bristow CS, Petts GE (eds), Blackwell: Oxford; 75–103.

Kleinhans MG, Jagers H, Mosselman E, Sloff C. 2008. Bifurcation dynamics and avulsion duration in meandering rivers by one-dimensional and three-dimensional models. *Water Resources Research* **44**. DOI:10.1029/2007WR005912.

Kleinhans MG, Cohen JM, Hoekstra J, IJmker JM. 2011. Evolution of a bifurcation in a meandering river with adjustable channel widths, Rhine delta apex, The Netherlands. *Earth Surface Processes and Landforms* **36**(15): 2011–2027.

Kleinhans MG, Ferguson RI, Lane SN, Hardy RJ. 2013. Splitting rivers at their seams: bifurcations and avulsion. *Earth Surface Processes and Landforms* **38**(1): 47–61.

Koch FG, Flokstra C. 1981. Bed level computations for curved alluvial channels. In *Proceedings of the XIX Congress of the International Association for Hydraulic Research*, Vol. 2, New Delhi; 357.

Koomen E. 1992. *Remote sensing study of morphological processes in the Jamuna River, Bangladesh*. MS thesis, Delft Hydraulics, Netherlands.

Leopold LB, Wolman MG. 1957. River channel patterns: braided, meandering and straight. *US Geological Survey Professional Papers* **282B**: 39–85.

Lesser GR, Roelvink JA, van Kester JATM, Stelling GS. 2004. Development and validation of a three-dimensional morphological model. *Coastal Engineering* **51**(8–9): 883–915.

Copyright © 2015 John Wiley & Sons, Ltd.

Lunt IA, Bridge JS, Tye RS. 2004. A quantitative, three-dimensional deposition model of gravelly braided rivers. *Sedimentology* **51**(3): 377–414.

Marra WA, Kleinhans MG, Addink EA. 2013. Network concepts to describe channel importance and change in multichannel systems: test results for the Jamuna River, Bangladesh. *Earth Surface Processes and Landforms* **39**(6): 766–778.

Meshkova LV, Carling PA. 2013. Discrimination of alluvial and mixed bedrock–alluvial multichannel river networks. *Earth Surface Processes and Landforms* **38**(11): 1299–1316.

Mosselman E. 2006. Bank protection and river training along the braided Brahmaputra-Jamuna River, Bangladesh. In *Braided Rivers: Process, Deposition, Ecology and Management*, Smith GHS, Best JL, Bristow CS, Petts GE (eds), Blackwell: Oxford; 277–287.

Mumpy AJ, Jol HM, Kean WF, Isbell JL. 2007. Architecture and sedimentology of an active braid bar in the Wisconsin River based on 3-d ground penetrating radar. *Geological Society of America Special Papers* **432**: 111–131.

Nicholas AP. 2003. Investigation of spatially distributed braided river flows using a two-dimensional hydraulic model. *Earth Surface Processes and Landforms* **28**(6): 655–674.

Nicholas AP. 2013a. Modelling the continuum of river channel patterns. *Earth Surface Processes and Landforms* **38**(10): 1187–1196.

Nicholas AP. 2013b. Morphodynamic diversity of the world's largest rivers. *Geology* **41**(4): 475–478.

Nicholas AP, Sandbach SD, Ashworth PJ, Amsler ML, Best JL, Hardy RJ, Lane SN, Orfeo O, Parsons DR, Reesink AJH, Sambrook Smith GH, Szupiany RN. 2012. Modelling hydrodynamics in the Rio Paraná, Argentina: an evaluation and inter-comparison of reduced-complexity and physics based models applied to a large sand-bed river. *Geomorphology* **169–170**: 192–211.

Rice SP, Church M, Wooldbridge CL, Hickin EJ. 2009. Morphology and evolution of bars in a wandering gravel-bed river: lower Fraser river, British Columbia, Canada. *Sedimentology* **56**(3): 709–736.

Roelvink JA. 2006. Coastal morphodynamic evolution techniques. *Coastal Engineering* **53**(2–3): 277–287.

Rozo MG, Noguiera ACR, Truckenbrodt W. 2012. The anastomising pattern and the extensively distributed scroll bars in the Middle Amazon River. *Earth Surface Processes and Landforms* **37**(14): 1471–1488.

Sambrook Smith GH, Ashworth PH, Best JL, Woodward J, Simpson CJ. 2006. The sedimentology and alluvial architecture of the sandy braided South Saskatchewan River, Canada. *Sedimentology* **53**(2): 413–434.

Schuurman F, Kleinhans MG, Marra WA. 2013. Physics-based modeling of large braided sand-bed rivers: bar pattern formation, dynamics, and sensitivity. *Journal of Geophysical Research* **118**(4): 2509–2527.

Struiksma N, Olesen K, Flokstra C, De Vriend H. 1985. Bed deformation in curved alluvial channels. *Journal of Hydraulic Research* **23**(1): 57–79.

Swinkels CM, Jeuken CMCJL, Wang ZB, Nicholls RJ. 2009. Presence of connecting channels in the Western Scheldt Estuary. *Journal of Coastal Research* **25**(3): 627–640.

Talmon AM, Struiksma N, Van Mierlo MCLM. 1995. Laboratory measurements of the direction of sediment transport on transverse alluvial-bed slopes. *Journal of Hydraulic Research* **33**(4): 495–517.

Van den Berg JH, Jeuken CJL, Van der Spek AJF. 1996. Hydraulic processes affecting the morphology and evolution of the Westerschelde estuary. In *Estuarine Shores: Evolution, Environment and Human Alterations*, Nordstrom KF, Roman CT (eds), Wiley: Chichester; 157–184.

Van der Mark CF, Mosselman E. 2012. Effects of helical flow in one-dimensional modelling of sediment distribution at river bifurcations. *Earth Surface Processes and Landforms* **38**(5): 502–511.

Van der Wegen M, Roelvink JA. 2008. Long-term morphodynamic evolution of a tidal embayment using a two-dimensional, process-based model. *Journal of Geophysical Research* **113**. DOI:10.1029/2006JF003983.

Van Dijk WM, Van de Lageweg WI, Kleinhans MG. 2012. Experimental meandering river with chute cutoffs. *Journal of Geophysical Research* **117**. DOI:10.1029/2011JF002314.

Wang Z, Fokkink R, de Vries M, Langerak A. 1995. Stability of river bifurcations in 1D morphodynamic models. *Journal of Hydraulic Research* **33**(6): 739–750.

Wheaton JM, Brasington J, Darby SE, Kasprak A. 2013. Morphodynamic signatures of braiding mechanisms as expressed through change in sediment storage in a gravel-bed river. *Journal of Geophysical Research* **118**: 759–779.

Zolezzi G, Bertoldi W, Tubino M. 2006. Morphological analysis and prediction of river bifurcations. In *Braided Rivers: Process, Deposition, Ecology and Management*, Smith GHS, Best JL, Bristow CS, Petts GE (eds), Blackwell: Oxford; 177–197.

Supporting Information

Supporting information may be found in the online version of this article at the publisher's web site.

Copyright © 2015 John Wiley & Sons, Ltd.